Human Molecular Genetics, 2013, Vol. 22, No. 14 **2881–2893**
doi:10.1093/hmg/ddt143
Advance Access published on April 4, 2013

Mutations in TFIIH causing trichothiodystrophy are responsible for defects in ribosomal RNA production and processing

Julie Nonnekens[1,2], Jorge Perez-Fernandez[3,4], Arjan F. Theil[5], Olivier Gadal[3,4] Chrystelle Bonnart[1,2,†] and Giuseppina Giglia-Mari[1,2,†,*]

[1]Centre national de la recherche scientifique (CNRS), Institute of Pharmacology and Structural Biology (IPBS), 205 route de Narbonne, Toulouse F-31077, France, [2]Université de Toulouse, UPS, IPBS, Toulouse F-31077, France, [3]CNRS, Le Laboratoire de Biologie Moléculaire Eucaryote (LBME), 118 route de Narbonne, Toulouse F-31062, France, [4]Université de Toulouse, UPS, LBME, Toulouse F-31077, France and [5]Department of Genetics, Erasmus MC, Dr Molewaterplein 50, Rotterdam 3015 GE, The Netherlands

Received January 29, 2013; Revised and Accepted March 27, 2013

The basal transcription/repair factor II H (TFIIH), found mutated in cancer-prone or premature aging diseases, plays a still unclear role in RNA polymerase I transcription. Furthermore, the impact of this function on TFIIH-related diseases, such as trichothiodystrophy (TTD), remains to be explored. Here, we studied the involvement of TFIIH during the whole process of ribosome biogenesis, from RNAP1 transcription to maturation steps of the ribosomal RNAs. Our results show that TFIIH is recruited to the ribosomal DNA in an active transcription-dependent manner and functions in RNAP1 transcription elongation through ATP hydrolysis of the XPB subunit. Remarkably, we found a TFIIH allele-specific effect, affecting RNAP1 transcription and/or the pre-rRNA maturation process. Interestingly, this effect was observed in mutant TFIIH-TTD cells and also in the brains of TFIIH-TTD mice. Our findings provide evidence that defective ribosome synthesis represents a new faulty mechanism involved in the pathophysiology of TFIIH-related diseases.

INTRODUCTION

During transcription, RNA polymerases, together with a large variety of supporting factors, engage in promoter binding, initiation, elongation and termination of transcription (1). One of those factors is transcription factor II H (TFIIH), a basal transcription complex essential for RNA polymerase II (RNAP2) transcription (2). TFIIH is comprised of 10 subunits that are divided in two sub-complexes (3). The core complex is formed by seven subunits (XPB, XPD, p62, p52, p44, p34 and TTDA), whereas the other three subunits (CDK7, MAT1 and cyclin H) form the cyclin-activating kinase complex, which is loosely bound to the core via the interaction with XPD (4). Besides functioning in RNAP2 transcription, TFIIH is also essential for nucleotide excision repair (NER). NER is a DNA repair pathway involved in the removal of helix-distorting lesions, during which the XPB and XPD helicases open the double-helix around the lesion to allow strand incision and repair of the damaged strand (5–7).

A decade ago, it was found that TFIIH plays a role in RNA polymerase I (RNAP1) transcription (8,9). Mass spectrometry analysis revealed the presence of TFIIH in the nucleolus, the site of RNAP1 transcription (10). Moreover, fractionation experiments showed that TFIIH could be isolated in complex with RNAP1 and the initiation factor TIF-IB (9). Although no precise function of TFIIH in RNAP1 transcription was revealed, different TFIIH resident times in RNAP1 and RNAP2 transcription suggested that TFIIH has a distinct function in these two processes (8). Indeed, in contrast to RNAP2 transcription, neither the ATPase, nor helicase, nor kinase activity of TFIIH appeared to be required for RNAP1 transcription initiation (9,11). Recently, it has been suggested that TFIIH plays a role during elongation of RNAP1 transcription (11). However, the mechanisms underlying TFIIH function in

*To whom correspondence should be addressed. Tel: +33 561175854; Fax: +33 5611759 94; Email: mari@ipbs.fr
†These two authors contributed equally.

RNAP1 elongation as well as the biological relevance for this novel function remain to be explored.

RNAP1 transcription is the first step of the finely orchestrated ribosome biogenesis process (12). Ribosome biogenesis is highly energy-consuming and involves the concerted actions of all three RNA polymerases and a large variety of transcription and maturation factors (13). RNAP1 is devoted to the transcription of the large 47S ribosomal DNA (rDNA), which is organized as head-to-tail tandem repeat sequences. The 47S sequence encodes for three of the four ribosomal RNAs (rRNAs: 18S, 5.8S and 28S) that are produced during intricate maturation and processing events involving more than 200 factors and snoRNAs (14). The rRNAs are assembled together with the 5S rRNAs (transcribed by RNA polymerase III) and ribosomal proteins to form the pre-ribosomal particles, which will be exported to the cytoplasm to form the final ribosome units (15).

Ribosome biogenesis is stimulated during cellular growth and high cellular metabolism, because fast-growing cells, such as cancer cells, require a high level of ribosome production to support rapid cellular division and protein production (16). The same need for a high ribosome production rate is found in neurons, which are metabolic active despite their post-mitotic state (17). Interestingly, skin abnormalities and neurological impairment are features found in a number of genetic diseases caused by mutations in ribosomal proteins or ribosomal factors (for example, ANE syndrome, characterized by alopecia, progressive neurological defects and endocrinopathy and diskeratosis congenita syndrome) (18). Moreover, the direct link between ribosome biogenesis and a human disease is strongly represented by Diamond–Blackfan anemia (DBA). Approximately 50% of the identified genetic defects in DBA patients are caused by mutations in genes encoding ribosomal protein subunits (19). The ribosomal protein S19 (RPS19) participates directly in the 18S rRNA maturation, and mutations found in the RPS19 gene causing DBA influence the production of the 40S ribosome subunit (20). Although the RPS19 protein is ubiquitously expressed, only specific cell types are affected in DBA patients, namely the erythroid precursors. This cell-type specificity shows that a subtle defect in ribosome production can affect the organism in a tissue-specific manner (21,22).

Mutations in TFIIH cause severe genetic disorders, xeroderma pigmentosum (XP) combined or not with Cockayne syndrome (XP/CS) and trichothiodystrophy (TTD and XP/TTD). XP is a cancer-prone skin disease, whereas CS and TTD are neurological syndromes presenting segmental premature aging features without cancer predisposition (23). The neurological abnormalities of both CS and TTD seem to be caused by hypomyelination. In CS, this is mainly triggered by a loss of myelin (demyelination), whereas in TTD, the defect would be attributed to a developmental defect (dysmyelination) (23). The functional complexity of TFIIH is illustrated by the existence of XP, TTD and the combined syndromes XP/CS and XP/TTD. This phenotypical variability cannot be attributed only to DNA repair defects, but could also be the consequence of TFIIH defects in transcription (24).

To gain a general view of the role of TFIIH in ribosome biogenesis, we investigated in detail the involvement of TFIIH in both rDNA transcription and the subsequent pre-rRNA maturation steps. Our results show that TFIIH binds all along the transcribed rDNA sequence, confirming the proposed role of TFIIH in RNAP1 transcription elongation (11). Moreover, we show that TFIIH is recruited to the rDNA in an active transcription-dependent manner and that ATP hydrolysis of the XPB subunit is important for enhancing RNAP1 transcription *in vivo*. Interestingly, RNAP1 transcription is altered in the TFIIH mutants Xpd^{TTD} and $Ttda^{-/-}$ and furthermore, a specific defect in the pre-40S maturation pathway was observed in Xpd^{TTD} mutant cells. This defect was found in cells but most importantly in brains obtained from the Xpd^{TTD} mouse model. Here, we propose a model for TFIIH functioning in RNAP1 transcription and thereby provide a new possible explanation for the neurodevelopmental defects observed in TTD patients.

RESULTS

TFIIH is involved in RNAP1 transcription elongation

It was previously shown that TFIIH can associate with a fraction of the RNAP1 transcription-competent form (9). Using fluorescent microscopy, we verified that TFIIH resides in the nucleolus at the site of RNAP1 transcription. Upon treatment with transcription inhibitors [5,6-dichloro-1β-D-ribofuranosyl benzimidazole and actinomycin D (ActD)], we found that TFIIH delocalization followed that of RNAP1 [Supplementary Material, Fig. S1 and (8)].

To investigate the role of TFIIH in RNAP1 transcription *in vivo*, we measured TFIIH and RNAP1 physical interactions with the rDNA by chromatin immunoprecipitation (IP) combined with quantitative PCR (ChIP–qPCR). In order to map the precise binding sites of RNAP1 and TFIIH on the rDNA, 14 different primer couples spanning along the rDNA sequence were designed for qPCR analysis (Fig. 1A).

The analysis of the RNAP1 binding profile on the rDNA (Fig. 1B and C) shows an increase of RNAP1 binding upstream of the transcription start site, indicating loading of RNAP1 on the rDNA at the promoter region. As predicted by its function, RNAP1 remains bound all along the transcribed region and is released upon termination. Identical to RNAP1 and the essential RNAP1 transcription factor, upstream binding factor (UBF) (25), TFIIH is associated with the rDNA throughout the transcribed region and is released upon termination.

The interaction of TFIIH with the rDNA coding sequences suggests its involvement throughout RNAP1 transcription elongation.

TFIIH recruitment to the rDNA is dependent on active transcription

To further study the recruitment of RNAP1 and TFIIH to the rDNA, we analyzed the binding of these factors in the absence of active RNAP1 transcription. ActD is a DNA intercalator which preferentially targets the GC-rich regions and stabilizes topoisomerase I (Topo 1), causing RNA polymerases to stop. Since the rDNA is rich in GC and RNAP1 transcription is highly dependent on Topo 1 activity, a low ActD

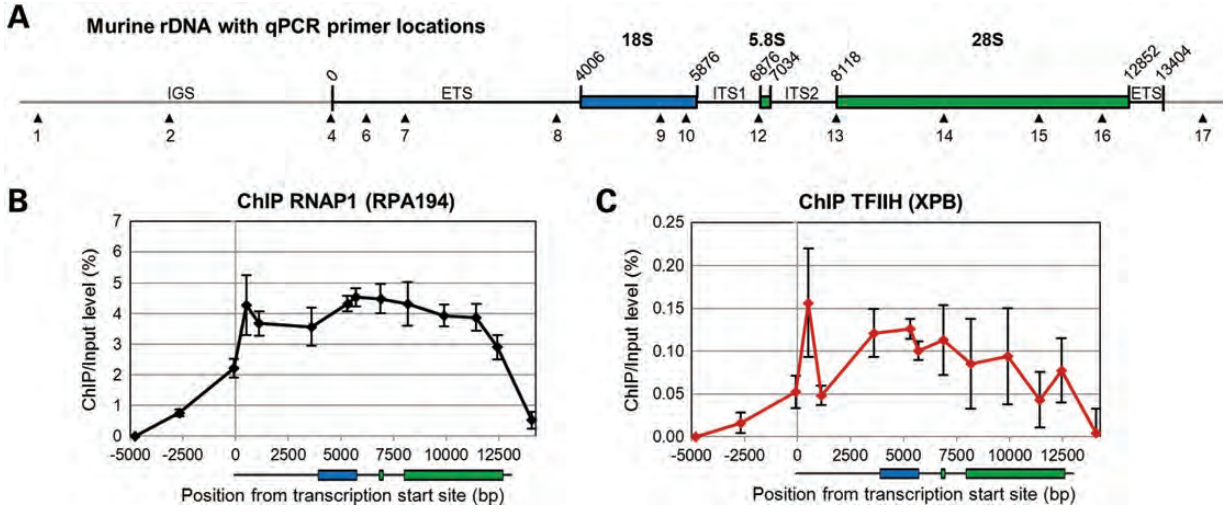

Figure 1. RNAP1 and the basal transcription/repair factor II H (TFIIH) binding to the rDNA genes. (**A**) Schematic representation of the murine rDNA unit. The coding regions of the 18S (blue), 5.8S and 28S (green) rDNA are illustrated and localizations of the primers used in the ChIP–qPCR analysis are depicted with arrowheads and numbers. IGS, intergenic spacer; ETS, external transcribed spacer; ITS, internal transcribed spacer. (**B** and **C**) ChIP–qPCR results showing the binding of (B) RNAP1 (black line) and (C) TFIIH (red line) to the transcribed and flanking regions of the murine rDNA. The *y*-axis represents the ChIP/input ratio minus background (mock/input ratio). Error bars represent the SEM of at least three independent experiments.

concentration inhibits RNAP1 transcription, but does not affect the other transcription processes in the cell (26).

To confirm the ActD-induced RNAP1 transcription inhibition in our assay, we measured the level of the 47S primary transcript (47S pre-rRNA) by northern blot (NB) and RNA fluorescence *in situ* hybridization (RNA FISH) experiments. After transcription, the 47S pre-rRNA transcript is rapidly processed and therefore its level is considered to be a reliable indicator for the rate of RNAP1 transcription (27). Both NB and RNA FISH use a probe targeting the 5′ end of the 47S pre-rRNA (Fig. 2A); the probe for RNA FISH is fluorescently tagged. The results show that 2 h of ActD treatment was sufficient to fully abolish RNAP1 transcription (Fig. 2B and C).

Following ActD treatment, RNAP1 accumulates on the rDNA promoter (primer 4), and RNAP1 binding along the rDNA genes is severely reduced (Fig. 2D). Surprisingly and in contrast to RNAP1, TFIIH does no longer bind to the rDNA promoter after treatment. Instead, a peak was detected immediately downstream of the transcription start site (Fig. 2E). This might indicate the formation of short-length rRNA transcripts, as previously described (26). In accordance with these results, we suggest that active transcription is strictly required for TFIIH recruitment on the rDNA.

ATP hydrolysis by XPB enhances RNAP1 transcription *in vivo*

Triptolide is the only known specific TFIIH inhibitor. *In vitro* studies have shown that triptolide binds directly to its subunit XPB and thereby inhibits the ATPase activity without affecting the helicase activity (28). In the same study, the authors found that NER and RNAP2 transcription were blocked by triptolide treatment, but *in vitro* RNAP1 transcription was not disturbed. However, this study did not provide evidence that the observed effects were also occurring *in vivo*. In order to investigate this, we measured the influence of triptolide on the RNAP1 and RNAP2 transcription levels in the cellular context. To measure RNAP1 transcription, we analyzed the accumulation level of the primary rRNA transcript by RNA FISH, whereas RNAP2 transcription was measured by 5-ethynyl uridine (EU) incorporation in the nucleoplasm. Our results show that triptolide rapidly inhibits RNAP2 transcription. Surprisingly and contrary to previous *in vitro* data (28), treatment with triptolide markedly reduced the level of the 47S pre-rRNA (Fig. 3A and C). Interestingly, treatment with the specific RNAP2 transcription inhibitor alpha-amanitin severely reduced RNAP2 transcription without affecting the production of the 47S primary transcripts (Fig. 3B and D). These results indicate that the effect of triptolide on RNAP1 transcription was not due to an indirect effect of reduced RNAP2 transcription. Altogether, the data indicate that XPB ATPase activity of TFIIH is required for efficient RNAP1 transcription *in vivo*.

We next examined the impact of triptolide on TFIIH and RNAP1 interactions with the rDNA using ChIP–qPCR (Fig. 3E). Our results reveal that the inhibition of the XPB ATPase activity modified the TFIIH binding to the rDNA. In fact, after triptolide treatment, TFIIH is released from the promoter and 5′ ETS region, but binds stronger to rDNA coding sequence (Fig. 3F). Interestingly, whereas the general binding profile of RNAP1 was unaffected, the quantity bound to the rDNA was significantly lower upon triptolide treatment (Fig. 3G).

Mutations in TFIIH and CSB affect RNAP1 binding to the rDNA

Since mutations in TFIIH cause severe human genetic diseases, we further examined the impact of clinically relevant TFIIH mutations on RNAP1 transcription. Like TFIIH, CSB (another NER protein) plays a role in RNAP1 transcription. Mutations in CSB cause CS phenotype, and cells harboring

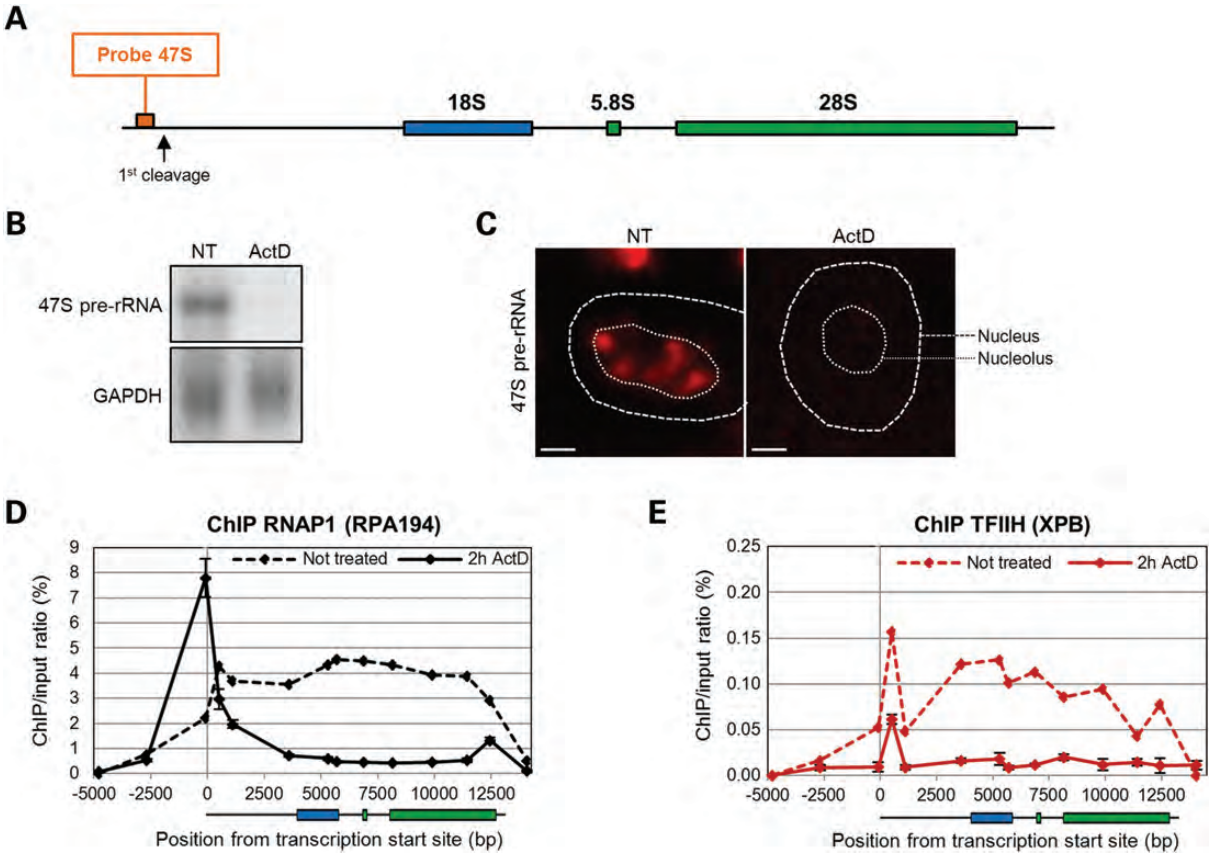

Figure 2. RNAP1 and TFIIH binding to the rDNA after ActD treatment. (**A**) Schematic representation of the murine rDNA unit and the position of the first maturation cleavage site. In orange, the location of the probe used for NB and RNA FISH is illustrated. (**B**) NB analysis showing the accumulation levels of the 47S pre-rRNA in ES cells untreated (NT) and treated for 2 h with ActD (ActD). GAPDH is used as a loading control. (**C**) RNA FISH (47S pre-rRNA) signals of ES cells untreated (NT) or treated for 2 h with ActD. RNA FISH shows the 47S pre-rRNA level of the nucleolus of one cell. Scale bars, 3 μm. (**D** and **E**) ChIP–qPCR results showing the binding of (D) RNAP1 (black line) and (E) TFIIH (red line) to the transcribed and flanking regions of the murine rDNA after 2 h treatment of ActD (solid lines) compared with untreated cells (dotted lines). The *y*-axis represents the ChIP/input ratio minus background (mock/input ratio). The error bars of the untreated curves (presented in Fig. 1) have been removed for a clearer overview and the error bars of the treated curves represent the SEM of three independent experiments.

a mutation in CSB have a reduced production of primary rRNA transcripts (29,30).

To investigate the impact of TFIIH and CSB mutations on RNAP1 transcription, we analyzed the RNAP1 binding to the rDNA in mutant cells. The cell lines used were isolated from $Csb^{-/-}$ [CS phenotype, mutation K337X in the *Csb* gene (31)], Xpd^{TTD} [TTD phenotype, mutation R722W in the *Xpd* gene (32)], $Ttda^{-/-}$ [deletion in the *Ttda* gene (A. Theil *et al*., accepted, PLoS Genet.)], Xpd^{XPCS} [XP/CS phenotype, mutation G602D in the *Xpd* gene (33)] and $Xpa^{-/-}$ (XP phenotype, deletion of two exons of the *Xpa* gene, see reference in Supplementary Material) mouse models.

As illustrated in Figure 4, we found an oscillation of the RNAP1 binding profile in $Csb^{-/-}$ and Xpd^{TTD} cells compared with wild-type (Fig. 4A and B). This effect was not found in Xpd^{XPCS} cells, in which the profile of binding was the same compared with wild-type littermate cells (Fig. 4D). Furthermore, in $Ttda^{-/-}$ cells, the overall RNAP1 binding is significantly lower than in wild-type cells (Fig. 4C). We used $Xpa^{-/-}$ cells (NER-deficient) to show that the observed effect was not due to the repair function of these proteins. As illustrated in Supplementary Material, Figure S2A, $Xpa^{-/-}$ cells do not have an altered binding of RNAP1 to the rDNA.

Furthermore, we analyzed the RNAP1 and UBF protein levels in whole-cell extracts of the mutant cells. Our results show that all cell lines have the same amount of RNAP1 and UBF (Fig. 4E and Supplementary Material, Fig. S2B), meaning that mutations in TFIIH or CSB have no impact on the RNAP1 and UBF protein steady-state levels. Therefore, our results show that RNAP1 binding modifications in the mutant cells were not due to an indirect effect of changes in the RNAP1 and UBF protein levels and favor a direct effect of the mutations on the RNAP1 binding to the rDNA genes.

TFIIH and CSB mutations impair RNAP1 transcription

Since the interaction of RNAP1 with the rDNA is affected in $Csb^{-/-}$, Xpd^{TTD} and $Ttda^{-/-}$ cells, we hypothesized that this could lead to a defective 47S pre-rRNA production. To verify this hypothesis, we analyzed the accumulation level of the 47S primary transcript by NB. Quantifications of the 47S pre-rRNA signals showed that the levels were significantly reduced by 50% in $Csb^{-/-}$, Xpd^{TTD} and $Ttda^{-/-}$ cells

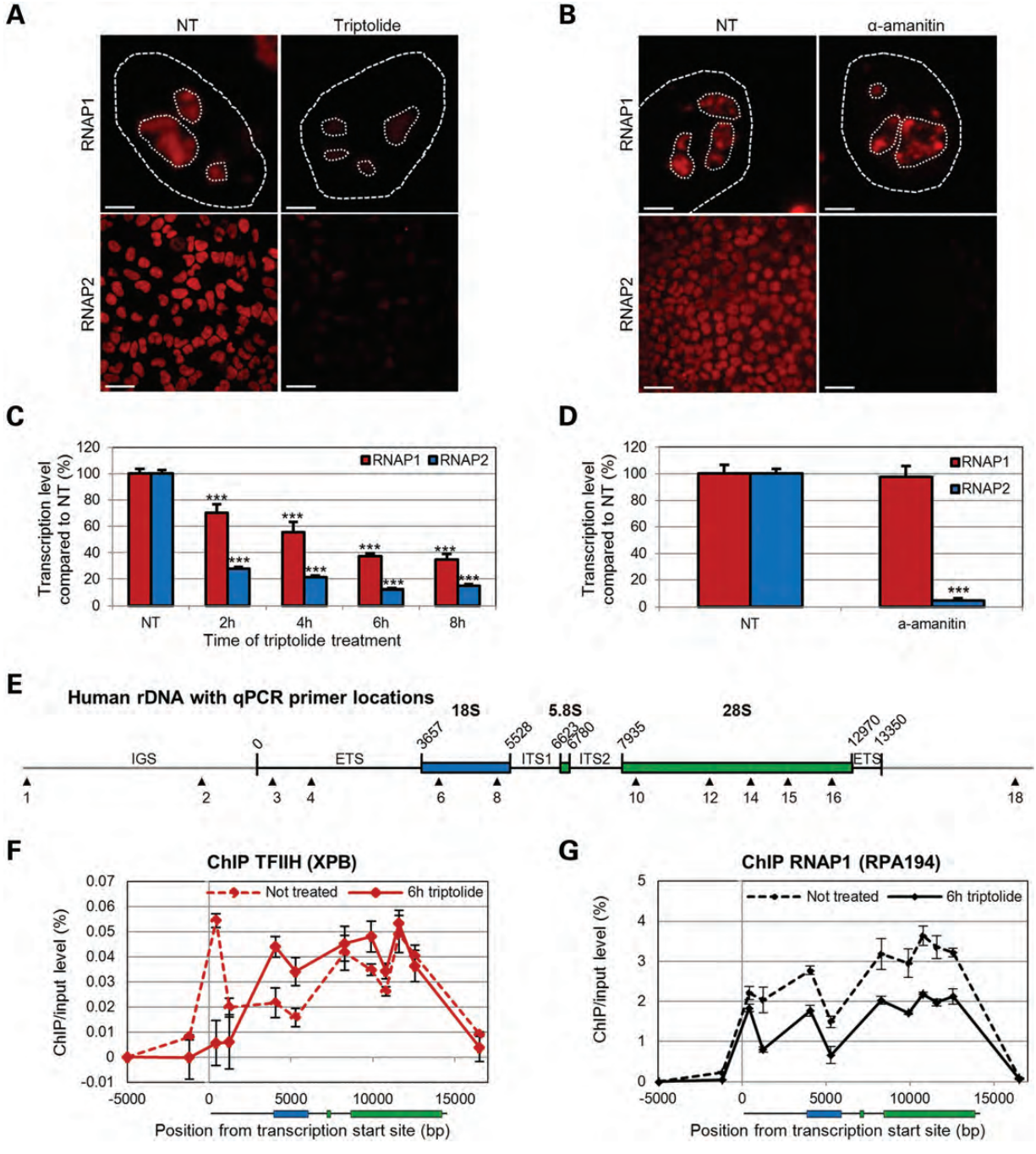

Figure 3. Influence of triptolide on RNAP1 transcription *in vivo*. (**A**) RNA FISH (RNAP1) and EU (RNAP2) signals of HeLa cells untreated (NT) or treated for 8 h with 10 μM triptolide. RNA FISH shows the 47S pre-rRNA level of the nucleoli of one cell, and EU incorporation is shown for a field of cells. Scale bars, 3 μm (RNAP1) and 30 μm (RNAP2). (**B**) RNA FISH (RNAP1) and EU incorporation (RNAP2) signals of HeLa cells untreated (NT) or treated for 16 h with 25 μg/ml alpha-amanitin. RNA FISH shows the 47S pre-rRNA level of the nucleoli of one cell, and EU incorporation is shown for a field of cells. Scale bars, 3 μm (RNAP1) and 30 μm (RNAP2). (**C**) The graph representing the quantification of the fluorescent pre-rRNA (red bars) and mRNA (blue bars) signals at different time points of triptolide treatment. (**D**) The graph representing the quantification of the fluorescent pre-rRNA (red bars) and mRNA (blue bars) signals of HeLa cells untreated (NT) or treated for 16 h with alpha-amanitin. (**E**) Schematic representation of the human rDNA unit. The coding regions of the 18S (blue), 5.8S and 28S (green) rDNA are illustrated and primer localizations (used in the ChIP–qPCR analysis) are depicted with arrowheads and numbers. IGS, intergenic spacer; ETS, external transcribed spacer; ITS, internal transcribed spacer. (**F** and **G**) ChIP–qPCR results showing the binding of (F) TFIIH (red line) and (G) RNAP1 (black line) to the transcribed and flanking regions of the human rDNA. The *y*-axis represents the ChIP/input ratio minus background (mock/input ratio). The untreated condition is shown as a dotted line and the curve after 6 h of treatment with triptolide as a solid line. $^{***}P < 0.001$ compared with NT. Error bars represent the SEM of at least three independent experiments.

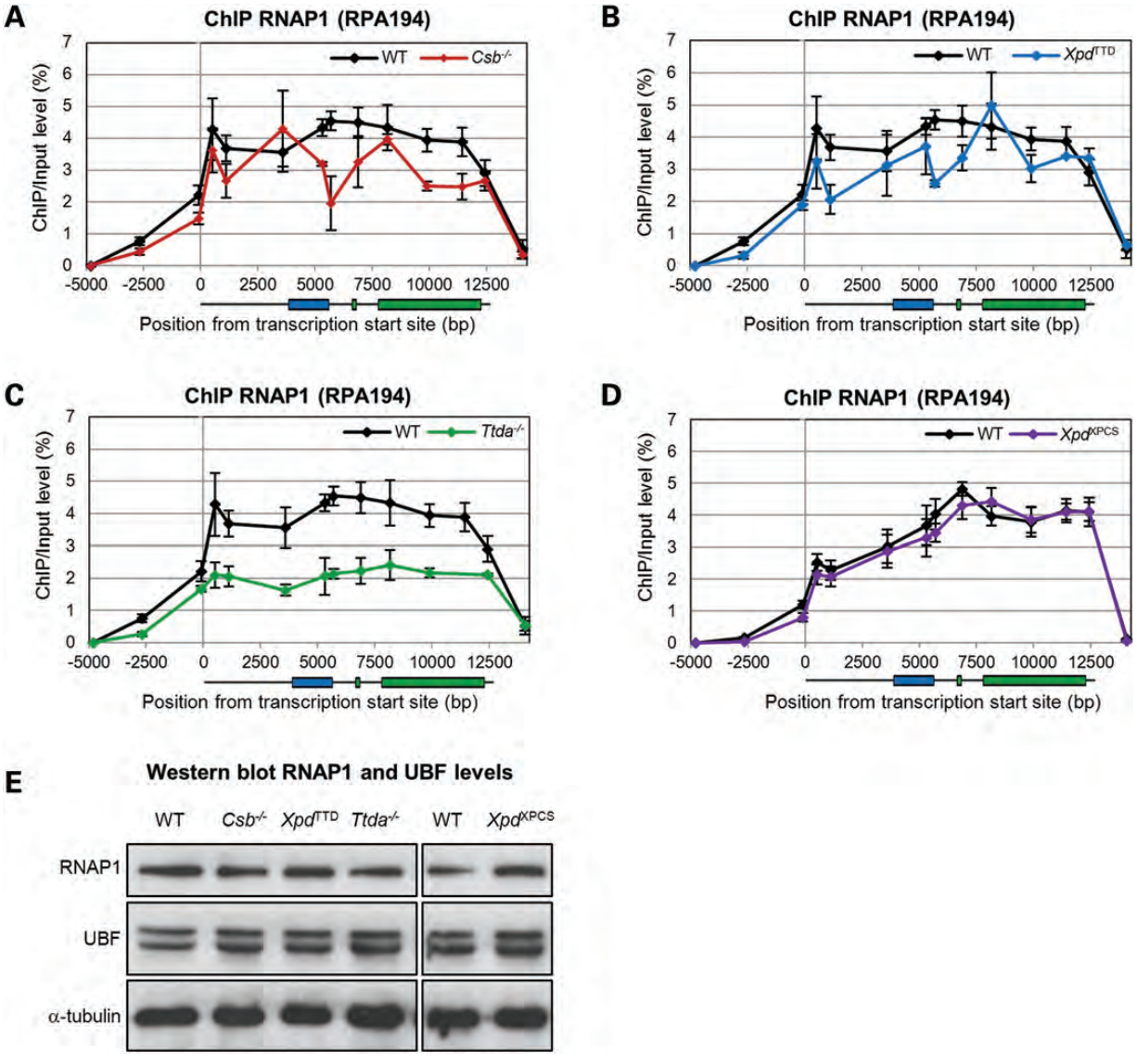

Figure 4. RNAP1 binding to rDNA is affected in CSB and TFIIH mutant cells. (**A**–**D**) ChIP–qPCR analysis of RNAP1 binding profile in (A) $Csb^{-/-}$ (red line), (B) Xpd^{TTD} (blue line), (C) $Ttda^{-/-}$ (green line) and (D) Xpd^{XPCS} (purple line) ES cells compared with wild-type (WT, black lines). The *y*-axis represents the ChIP/input ratio minus background (mock/input ratio). Error bars represent the SEM of at least three independent experiments. (**E**) Western blot of whole-cell extracts of wild-type (WT) and mutant ES cells. RNAP1 blot (upper panel) and UBF blot (middle panel) were compared with the α-tubulin blot, used as a loading control (lower panel).

compared with wild-type. Interestingly, in Xpd^{XPCS} and $Xpa^{-/-}$ cells, the amount of 47S pre-rRNA was not reduced (Fig. 5A and B, Supplementary Material, Fig. S2C and D), which is consistent with the normal RNAP1 binding profile in these mutants. To verify these NB results *in situ*, we performed RNA FISH experiments. Consistent with the NB results, the 47S pre-rRNA quantity was significantly decreased in the $Csb^{-/-}$, Xpd^{TTD} and $Ttda^{-/-}$ cells (Fig. 5C and D). We further analyzed the RNAP1 transcription levels by pulse labeling. The rRNA is co-transcriptionally methylated and incorporation of L-methyl-^{3}H-methionine can therefore be used to study the kinetics of RNAP1 transcription (34). We verified that the level of fibrillarin, the enzyme driving pre-rRNA methylation, was similar among our different embryonic stem (ES) cell lines, to exclude the possibility of variable methylation levels among the ES cell lines (Supplementary Material, Fig. S3D). Pulse labeling confirmed the results obtained previously, showing a significant decrease in the production of the 47S pre-rRNA in $Csb^{-/-}$, Xpd^{TTD} and $Ttda^{-/-}$, but not in Xpd^{XPCS} cells (Supplementary Material, Fig. S3B and C).

Taken together, we conclude that some of the TFIIH mutations (but not all) impede proper binding of RNAP1 to the rDNA as well as correct production of the 47S pre-rRNA.

Pre-rRNA maturation is affected in Xpd^{TTD} mutant cells

During its production and shortly thereafter, the pre-rRNA undergoes several modifications and is subsequently cleaved into different intermediates until the mature rRNAs are formed (Fig. 6A) (35). Since RNAP1 transcription and

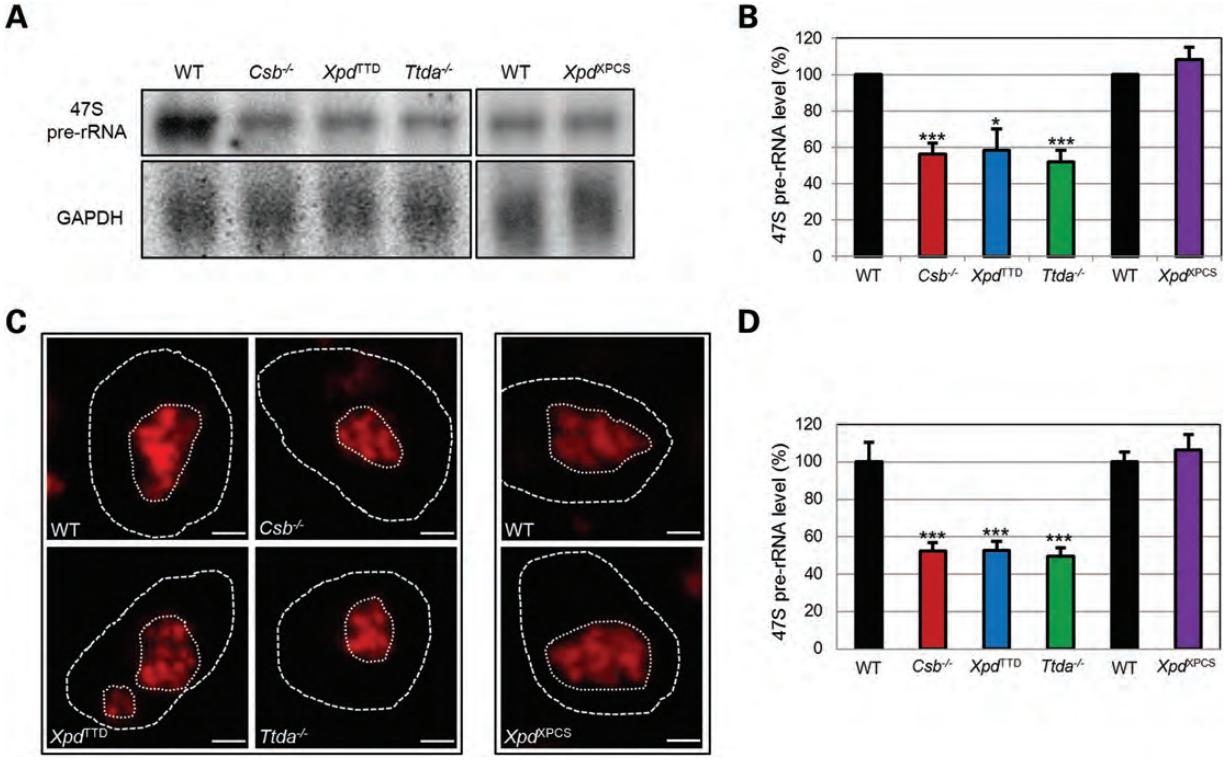

Figure 5. RNAP1 transcription is reduced in CSB and TFIIH mutant cells. (**A**) NB analysis showing the accumulation levels of the 47S pre-rRNA in wild-type (WT), $Csb^{-/-}$, Xpd^{TTD}, $Ttda^{-/-}$ and Xpd^{XPCS} ES cells. GAPDH is used as a loading control. (**B**) Quantifications of the NB signals of three independent experiments illustrated in (A). (**C**) RNA FISH signal of the 47S pre-rRNA in WT, $Csb^{-/-}$, Xpd^{TTD}, $Ttda^{-/-}$ and Xpd^{XPCS} ES cells. Scale bars, 3 μm. Images of extra cells can be found in Supplementary Material, Figure S3A. (**D**) Quantification of the RNA FISH signals, showing the average fluorescence level of the nucleoli of 10 cells for each condition compared with WT. $^{*}P < 0.05$ and $^{***}P < 0.001$ compared with WT. Error bars represent the SEM of three independent experiments.

maturation are closely linked (36), we questioned whether the maturation process in TFIIH-mutated cells would also be affected. For that, we analyzed total RNA by NB using probes that target the various pre-rRNA intermediates (Fig. 6A and B). Using the 5′ ITS1 probe, we observed a high amount of the 34S pre-RNA level specifically in the Xpd^{TTD} cells. The 18S-E/34S ratio, which is an internal measure for the pre-40S ribosomal pathway, was significantly decreased in these cells compared with control cells (Fig. 6C), indicating that Xpd^{TTD} cells are impaired in one or multiple cleavages in the pre-40S pathway. These results show an unprecedented allele-specific effect of the Xpd^{TTD} mutation on rDNA transcription and subsequent pre-rRNA maturation.

The Xpd^{TTD} mouse model shows a transcription and pre-rRNA maturation defect in adult brains

We have shown that RNAP1 transcription and the pre-40S ribosome biogenesis pathway were impaired in ES cells carrying an allele-specific mutation in *Xpd*, which drives the TTD phenotype *in vivo*. Remarkably, TFIIH is present at a very high level in the nucleolus of metabolically active neurons (37) and it is worth to be noted that TTD patients and Xpd^{TTD} mutant mice display neurological abnormalities. We therefore examined whether a ribosome biogenesis defect could be found in the brain of TTD mice.

Total RNA isolated from brains of 3-month-old Xpd^{TTD}, Xpd^{XPCS} and wild-type mice was analyzed by NB. Quantification of the NB signals from biological triplicates revealed a significant decrease of the 47S pre-rRNA level in Xpd^{TTD} brains, similar to the corresponding ES cells. Brain analysis from Xpd^{XPCS} mice, however, did not show a significant decrease in RNAP1 transcriptional activity (Fig. 7A and B). Importantly, the 18S-E/34S rRNA ratio was significantly reduced in Xpd^{TTD} brains, but not in Xpd^{XPCS} brains (Fig. 7C and D). This indicates that, like in undifferentiated ES cells, a ribosome maturation defect in the pre-40S pathway is present in the brain of Xpd^{TTD} mice. Moreover, this defect appears specific to the TTD phenotype since ribosomal biogenesis remains normal in the brain of Xpd^{XPCS} mice.

DISCUSSION

The role of TFIIH in DNA repair and RNAP2 transcription has been extensively described. A decade ago, a new function of TFIIH in RNAP1 transcription was suggested (8,9). After this finding, an additional study reinforced this principal observation and proposed a role of TFIIH in the production of full-length rRNA transcripts by enhancing the elongation step of the RNAP1 transcription cycle (11). Nevertheless, the exact mechanism of action of TFIIH in RNAP1 transcription remains to be explored. Most importantly, no clear link was found between this new function and the distinct

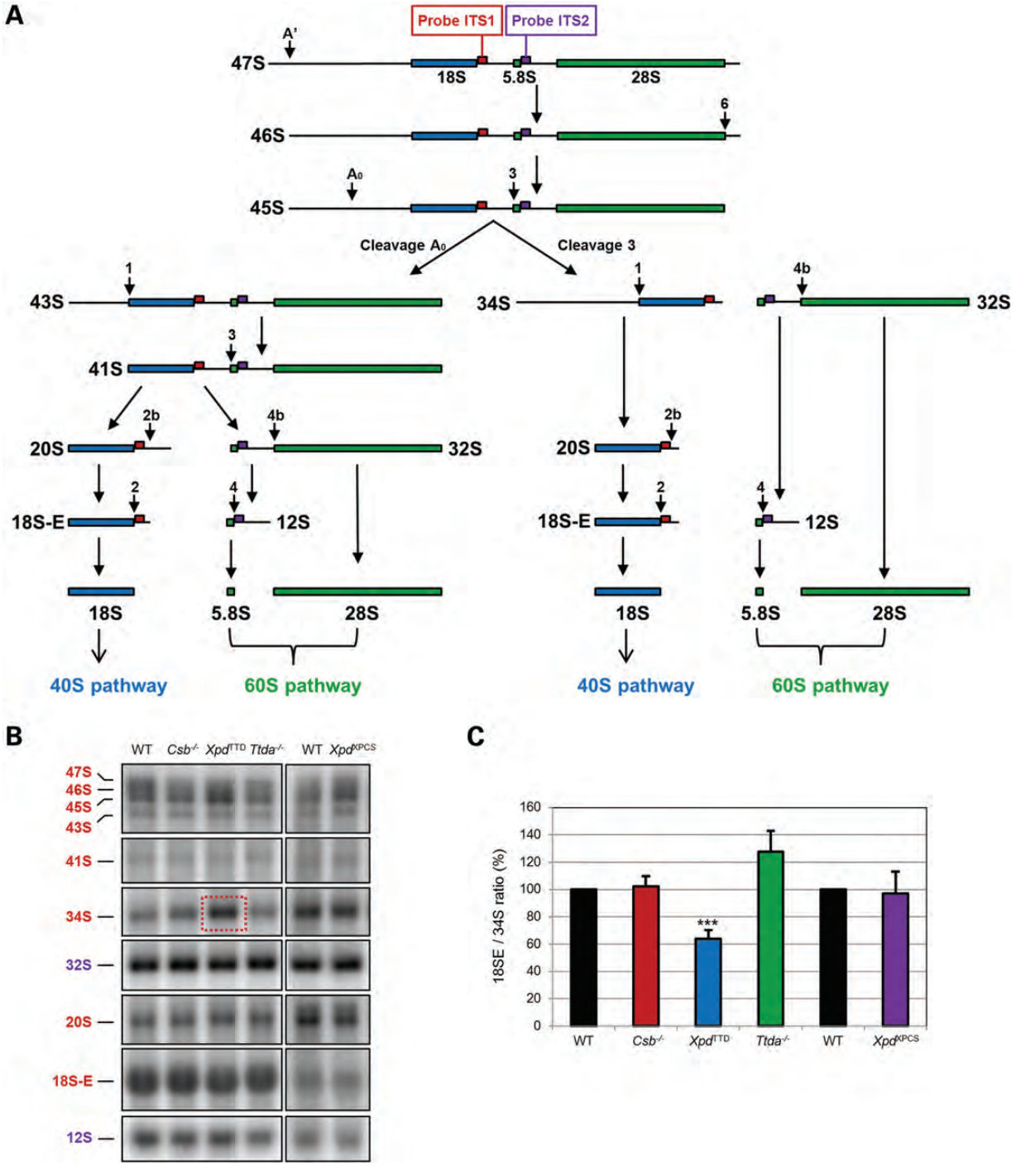

Figure 6. *Xpd*^{TTD} cells show a specific 40S pre-rRNA maturation defect. (**A**) Outline of the pre-rRNA processing pathway in murine cells; adapted from Mullineux and Lafontaine (35). The locations of the two probes used in the NB analysis are depicted by red and purple boxes (5′ ITS1 probe and ITS2 probe). (**B**) NB showing the accumulation levels of the different pre-rRNA species in wild type, *Csb*$^{-/-}$, *Xpd*^{TTD}, *Ttda*$^{-/-}$ and *Xpd*^{XPCS} ES cells. Red and purple color code is used to differentiate the species recognized by 5′ ITS1 and ITS2 probes, respectively. (**C**) Quantifications of three independent experiments of the 18S-E/34S ratio (40S pathway) compared with wild type. $^{***}P < 0.001$ compared with WT. Error bars represent the SEM of three independent experiments.

mutations in TFIIH that cause phenotypically diverse, severe genetic disorders. In this study, for the first time, we reveal the specific alteration of rRNA production in some but not all mutated forms of TFIIH in both cell lines and murine brains.

We established a very detailed binding profile of TFIIH and RNAP1 all along the coding region of the mammalian rDNA genes. Our results strengthen the suggestion of Assfalg *et al.* (11) that gives to TFIIH a function in RNAP1 post-initiation steps, and more precisely RNAP1 transcription elongation,

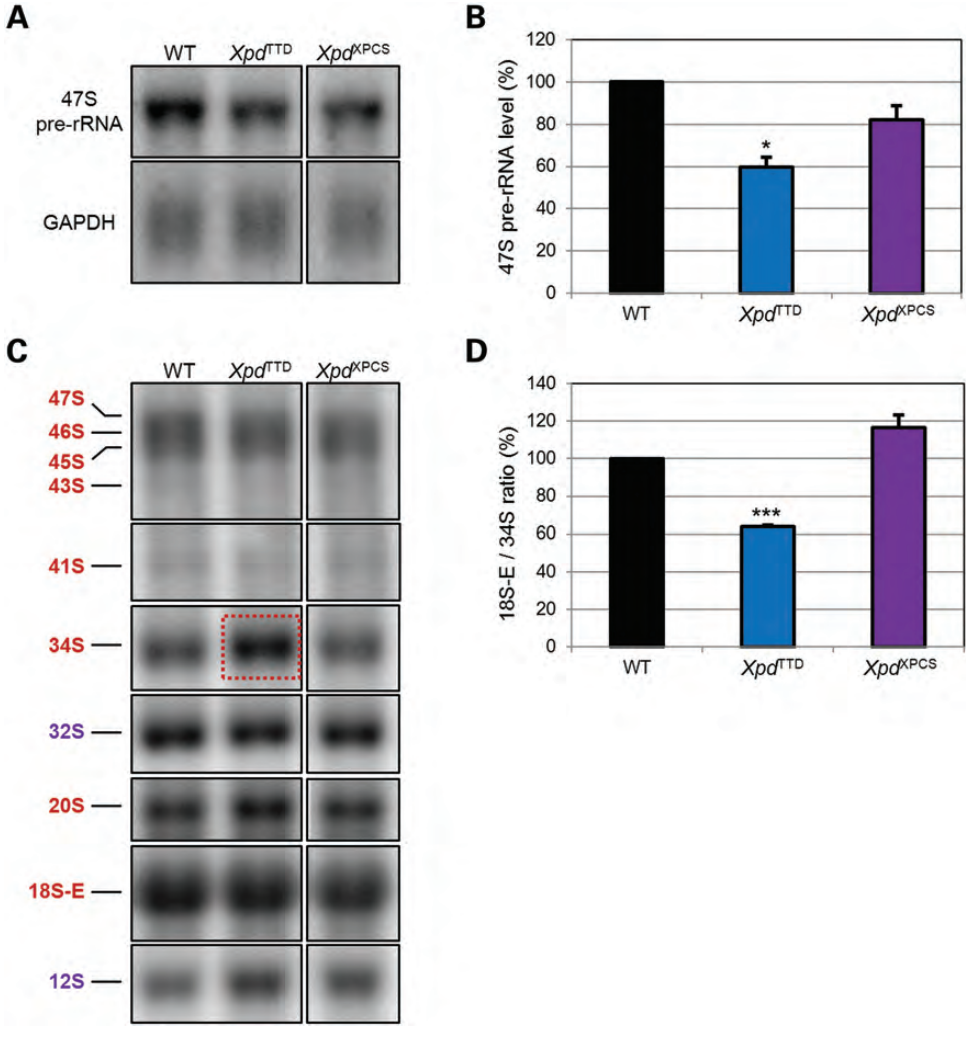

Figure 7. RNAP1 transcription levels and pre-rRNA maturation profiles are affected in Xpd^{TTD} murine brains. (**A**) NB analysis showing the accumulation levels of the 47S pre-rRNA in wild-type, Xpd^{TTD} and Xpd^{XPCS} murine brains. GAPDH is used as a loading control. (**B**) The bar graph represents the quantification of the 47S/GAPDH ratio of three different brains compared with wild-type. (**C**) NB analysis showing the accumulation levels of the different pre-rRNA species in control, Xpd^{TTD} and Xpd^{XPCS} murine brains. (**D**) The graph represents the quantification of three different brains of the 18S-E/34S ratio (40S pathway) compared with control. $^{*}P < 0.05$ and $^{***}P < 0.001$ compared with WT. Error bars represent the SEM of three independent experiments.

as well as give a detailed overview of the binding behavior of TFIIH to the rDNA. Many assets of RNAP1 transcription are conserved in different species such as yeast and higher eukaryotes. Previously, it was shown that yeast strains carrying temperature-sensitive mutations in TFIIH have a reduced production of the 35S pre-rRNA primary species (9). We have examined the binding of RNAP1 and TFIIH to the rDNA of the yeast *Saccharomyces cerevisiae*. Our results show that, in yeast, TFIIH binds to the rDNA all along the transcribed region like in mammalian cells (Supplementary Material, Fig. S4). These results indicate that the participation of TFIIH in RNAP1 transcription elongation is an evolutionary conserved process. Importantly, our results demonstrate that TFIIH is detected throughout the transcribed region of the mammalian and yeast rDNA and is loaded at the transcriptional start site.

In contrast to previous data (11), our results clearly show that blocking of RNAP1 transcription with ActD impedes TFIIH binding to the rDNA *in vivo*, indicating that TFIIH binds in an active transcription-dependent manner. In fact, after ActD treatment, RNAP1 can still bind to the promoter, whereas TFIIH does not bind anymore, suggesting that RNAP1 binding precedes TFIIH binding. By using the TFIIH-specific inhibitor triptolide (28), we examined whether blocking the TFIIH-XPB ATPase activity has a consequence on RNAP1 transcription. Triptolide treatment reduced the overall amount of RNAP1 bound to the coding rDNA, without affecting its general binding profile. Interestingly, RNAP1 binding at the promoter was not changed. On the contrary, the TFIIH binding profile was significantly affected at the transcriptional start site by the inhibition of its ATPase activity. These observations suggest that the ATPase activity of XPB is dispensable for RNAP1 promoter binding, but that binding of TFIIH in this region is important for proper RNAP1 transcription. The effect of triptolide on RNAP1 transcription was most likely due to a direct effect of TFIIH on

RNAP1 transcription instead of an indirect RNAP2 transcription defect, since RNAP2 transcription inhibition by alpha-amanitin did not result in the reduction of the 47S primary transcript. Additionally, the triptolide treatment did not cause variations in RNAP1 or XPB protein levels as shown in Supplementary Material, Figure S5. In summary, we demonstrate here that the ATPase function of TFIIH (XPB) is important for the maintenance of correct interaction between TFIIH and RNAP1 with the rDNA and consequently for proper transcription. Titov *et al*. (28) showed that triptolide does not inhibit RNAP1 transcription *in vitro*. Nevertheless, our data show that in the living cell, in the context of chromatin, triptolide is able to block RNAP1 transcription. This result can suggest that TFIIH improves the transcription reaction by supplying energy for chromatin conformational changes, most likely during early elongation.

Remarkably, the TFIIH binding profile differs from the one observed for RNAP1. RNAP1 displays a processive profile, whereas the one of TFIIH seems to be distributive. This result is in accordance with previously measured residence times of both TFIIH and RNAP1. In fact, it has been shown that during RNAP1 transcription, the residence time of elongating RNAP1 is ∼140 s (38), whereas TFIIH is estimated to be engaged only for 25 s in this process (8). Based on these observations, we suggest that TFIIH could shuttle on and off the rDNA during transcription elongation and we can propose that for one RNAP1 reaction, TFIIH would bind five separate times. The shuttling capacity of TFIIH is in agreement with the model proposed by Hoogstraten *et al*. (8), where TFIIH is in equilibrium between the transcription functions (RNAP2 and RNAP1) and the DNA repair engagements.

Several genetic diseases are caused by mutations in the TFIIH-encoding genes and despite decades of research on TFIIH, the correlation between genotype and phenotype is still poorly understood. Therefore, we examined the impact of clinically relevant TFIIH mutations on RNAP1 transcription and further steps in ribosome biogenesis. Remarkably, our results show a modification of RNAP1 binding to the rDNA in $Csb^{-/-}$, Xpd^{TTD} and $Ttda^{-/-}$ cells, but not in Xpd^{XPCS} cells. RNase treatment did not affect the general binding profile of RNAP1 in Xpd^{TTD} cells (data not shown), meaning that the difference of profile is probably not due to accumulation of unprocessed or partially processed transcripts which perturb the reaction. Specifically in $Ttda^{-/-}$ cells, the overall RNAP1 binding level was significantly lower compared with wild-type cells. This alteration is similar to the one observed after transcription inhibition with triptolide. The fact that TTDA stimulates the XPB ATPase activity (39) and that the same alteration of the binding of RNAP1 in both $Ttda^{-/-}$ and triptolide-treated cells was observed suggest yet again that the XPB ATPase activity is important for proper RNAP1 transcription. In agreement with the altered binding profiles, we showed a clear reduction of the 47S pre-rRNA transcript formation in the $Csb^{-/-}$, Xpd^{TTD} and $Ttda^{-/-}$ cells, but not in Xpd^{XPCS} cells. The allele-specific effect of mutations in *Xpd* might be explained by the fact that mutations in TFIIH change the conformation of the complex, but all in a different manner (40). Therefore, it is probable that only the Xpd^{TTD} mutation has an impact on the TFIIH conformation that affects its function in RNAP1 transcription.

All phases of ribosome biogenesis are coordinated and defined in space and time, and optimal RNAP1 transcription requires the physical presence of the pre-rRNA processing machinery (36), meaning that RNAP1 transcription and rRNA maturation should be considered as two coupled processes (41). Furthermore, the close relation between transcription elongation and maturation is illustrated by Schneider *et al*. (42), who show that a defect in RNAP1 transcription elongation in yeast leads to a defect in the pre-rRNA maturation. Interestingly, we observed a clear and specific impairment of the pre-40S ribosomal maturation pathway in the Xpd^{TTD} cells. This defect and the transcription defect were not only observed in the Xpd^{TTD} mutant cells, but also in the brains originating from Xpd^{TTD} mice, indicating that TFIIH defects in ribosome biogenesis are conserved throughout development. Since ribosome production is a prominent process in neurons (17), this specific defect could be highly detrimental to neuronal activity in TTD patients and therefore could be at least partly involved in TTD pathophysiology. Interestingly, neurological abnormalities are a feature found in a number of ribosomopathies.

Altogether, we show here that TFIIH is involved in RNAP1 transcription elongation *in vivo* and that the XPB ATPase activity is an enhancing factor of this activity. We furthermore demonstrate that TFIIH is loaded onto the rDNA at the level of the transcription start site in an active transcription-dependent manner. In addition to these new insights into the molecular mechanisms of TFIIH occupancy in RNAP1 transcription, we shed light on the impact of clinically relevant mutations of TFIIH and CSB on the production of the primary rRNA transcripts and subsequent post-transcriptional steps involved in ribosomal particle formation. Remarkably, we show, for the first time, an allele-specific effect of mutations in TFIIH on rDNA transcription and pre-rRNA maturation in both cells and the brain of a TFIIH mouse model. Our findings strongly suggest that TTD neurological features could be in some extent due to the impairment of ribosome biogenesis, in addition to other proposed abnormalities in hormone-related transcription and repair mechanisms (43,44). This allele specificity emphasizes the complexity underlying each phenotype of TFIIH-associated disorders, in particular the neurological symptoms affecting CS and TTD patients.

MATERIALS AND METHODS

Ethics statement

All experiments involving living animals have been conducted according to Federation of European Laboratory Animal Science Associations (FELASA) ethical requirements and according to the 3R animal welfare rules.

Origin of ES cells and mouse models

Mutant ES cells ($Csb^{-/-}$, Xpd^{TTD} and $Ttda^{-/-}$) were used in this study together with their corresponding ES Xpb^{YFP} as a control line (ES WT). Mutant ES Xpd^{XPCS} and ES cells

derived from a wild-type Xpd^{XPCS} littermate were used as a control line. These cells were isolated from the following mouse model: the XPB-YFP mouse model (Xpb^{YFP}), created as previously described (37). This mouse model was crossed with several mutant mouse models to obtain double homozygotes. Model $Xpb^{YFP}{\cdot}Csb^{-/-}$ (hereafter $Csb^{-/-}$) harbors a mutation in CSB causing a C-terminal deletion (K337→stop), mimicking the CS-B patient mutation (31). Model $Xpb^{YFP}{\cdot}Xpd^{TTD}$ (hereafter Xpd^{TTD}) harbors a mutation in XPD at position 722 (XPDR722W), mimicking the XPD-TTD patient mutation (32). Model $Xpb^{YFP}{\cdot}Ttda^{-/-}$ (hereafter $Ttda^{-/-}$) has a deletion of the coding region of TTDA (A. Theil *et al*., accepted, PLoS Genet.). Model Xpd^{XPCS} (without Xpb^{YFP}) harbors a mutation in XPD at position 602 (XPDG602D), mimicking the XPD-XP/CS patient mutation (33).

For NB experiments, brains from the Xpd^{TTD} mice, Xpd^{XPCS} mice and littermate control mice were analyzed.

Cell culture and treatment

ES cells were cultured in a 1:1 mixture of Dulbecco's modified Eagle's medium (DMEM) (Lonza) and BRL-conditioned medium, supplemented with 1% antibiotics (Lonza), 10% fetal bovine serum (Gibco), non-essential amino acids (Gibco), β-mercaptoethanol (Sigma) and leukemia inhibitory factor. HeLa cells were cultured in DMEM, supplemented with 1% antibiotics and 10% fetal bovine serum. All cells were incubated at 37°C with 5% CO_2.

For transcription inhibition, cells were incubated in regular medium containing ActD (Sigma, 0.1 μg/ml for 2 h), triptolide (Sigma) (10 μM for 2, 4, 6 or 8 h) or alpha-amanitin (25 μg/ml for 16 h).

ChIP on ES and HeLa nuclear extracts

ES and HeLa cells were grown in 14.5 cm culture dishes. Cells were fixed with 1% formaldehyde (Sigma) in PBS for 10 min (min) at room temperature and crosslinking was stopped by adding glycine (0.125 M final). Cells were harvested by scraping in PBS and pelleted by centrifugation. Cell lysis was performed with lysis buffer (50 mM HEPES–KOH, pH 8, 1 mM EDTA, 500 mM NaCl, 10% glycerol, 0.5% NP-40, 0.25% Triton X-100 and protease inhibitors), and incubated for 10 min at 4°C. Nuclei were pelleted by centrifugation and washed with wash buffer (10 mM Tris–HCl, pH 8, 1 mM EDTA, 500 mM NaCl and protease inhibitors), and incubated for 10 min at 4°C. Washed nuclei were pelleted by centrifugation, resuspended in IP buffer (50 mM HEPES–KOH, pH 7.5, 1 mM EDTA, 500 mM NaCl, 1% Triton X-100, 0.1% Na-deoxycholate, 0.1% SDS and protease inhibitors) and sonicated in a Bioruptor UDC-200 (Diagenode, set up high for 30 min, with cycles of 30 s on/1 min off) to yield DNA fragments with an average size of 300 bp. Samples were centrifuged at 14 000*g* for 5 min to remove insoluble material and measured with a nanodrop at 260 nm. Optimal amounts of ES and HeLa extracts to maximize ChIP/input ratio were incubated overnight at 4°C in 150 μl of total volume with the different antibodies (ChIP) or no antibody (mock). Antibodies used were anti-RNAP1 (RPA194 C-1 Santa Cruz), anti-HA (16B12 Eurogentec) (ChIP TFIIH, ES) or anti-XPB (p89 S-19 Santa Cruz) (ChIP TFIIH, HeLa). IP was performed for 1 h at 4°C with 40 μl of washed magnetic Bio-Adembeads Protein G (Ademtech). After IP, the beads were washed two times with IP buffer, once with Na-deoxycholate buffer (10 mM Tris–HCl, pH 8.0, 1 mM EDTA, 250 mM LiCl, 0.5% NP-40 and 0.5% Na-deoxycholate) and once with TE buffer (50 mM Tris–HCl, pH 8.0, and 10 mM EDTA). DNA and proteins were eluted with an elution buffer (50 mM Tris–HCl, pH 8.0, 10 mM EDTA and 1% SDS) by incubation for 20 min at 37°C. DNA from ChIP, mock and input preparations was decrosslinked and purified by phenol–chloroform extraction. Samples were quantified by real-time PCR using the Power SYBR Green PCR master mix (Applied Biosystems) on a 7300 Real-Time PCR System (Applied Biosystems). In order to take copy number into account, ChIP data were normalized to the input and subtracted to the background (mock). Biological replicates were generated for each experiment. Primer sequences for qPCR can be found in the Supplementary Material.

RNA extraction of cells and murine brains

Extractions of total RNAs from cells were performed using TRIzol reagent (Invitrogen). Cells were trypsinized and washed in PBS. The pellet was resuspended in 1 ml of TRIzol and processed as recommended by the manufacturer. Harvested brains were cut in four parts and homogenized in 5 ml of TRIzol using a douncer. An amount of 1 ml of the brain/TRIzol mixture was centrifuged to remove insoluble material and the supernatant was subjected to RNA extraction as described by the manufacturer.

Northern blot

The NB protocol was adapted from Sambrook and Russell (45). Briefly, 4 μg of total RNA was separated on a 1.2% agarose gel. RNAs were transferred to Amersham Hybond N+ membranes (GE Healthcare) which were hybridized with ^{32}P-labeled oligonucleotides using Rapid-hyb buffer (GE Healthcare). The membranes were exposed to Phosphor Screens, which were developed in the PhosphorImager apparatus and quantified with the use of the ImageQuant software. The sequences of the oligonucleotides used as probes in this study are described in the Supplementary Material.

RNA FISH

Cells were grown on 12 mm coverslips, washed with PBS and fixed with 4% paraformaldehyde for 20 min at 37°C. Cells were permeabilized with PBS 0.4% Triton X-100 for 10 min at 4°C and incubated with prehybridization buffer (2× SSPE and 15% formamide) (20× SSPE, pH 8.0: 3 M NaCl, 157 mM $NaH_2PO_4{\cdot}H_2O$ and 25 mM EDTA). An amount of 1.5 μl of probe (10 ng/μl) was diluted in 30 μl of hybridization mix (2× SSPE, 15% formamide, 10% dextran sulfate, 0.5 mg/ml tRNA) and heated to 90°C for 1 min. Hybridization of the probe to the cells was conducted overnight at 37°C in a humid environment. Coverslips were washed two times for 20 min with prehybridization buffer and one time for 20 min with 1× SSPE and then mounted with Vectashield (Vector).

The sequences of the oligonucleotides used as probes can be found in the Supplementary Material. At least 10 different cells were quantified for each condition.

mRNA detection

Cells were grown on 12 mm coverslips and treated or not with triptolide. The mRNA detection was performed using a Click-iT RNA Alexa Fluor Imaging Kit, according to the manufacturer's protocol (Invitrogen). The fluorescence signal of the nucleoplasm of 60 different cells was quantified for each condition.

Fluorescent imaging and analysis

Imaging has been performed at high time resolution on a Zeiss LSM 710 NLO confocal laser scanning microscope (Zeiss), using a 40/1.3 oil objective. Images were analyzed with the ImageJ software.

Protein extraction and western blot

ES or HeLa cells were grown on 6 cm culture dishes and harvested by trypsinization. Cells were lysed with 200 μl of ProteoJET Mammalian Cell Lysis Reagent (Fermentas) according to the manufacturer's protocol. An amount of 25 μg of protein was loaded on an 8% SDS–PAGE and transferred to a nitrocellulose membrane (Whatman). Membranes were blocked for 1 h in 5% milk in PBS 0.1% Tween and subsequently incubated overnight with the different primary antibodies [anti-RNAP1 (RPA194 C-1, Santa Cruz), anti-UBF (F-9 Santa Cruz), anti-XPB (p89 S-19, Santa Cruz), anti-fibrillarin (provided by the Henry-Henras team, IBCG, Toulouse, France) and anti-tubulin (B-5-1-2, Sigma)]. Membranes were then incubated with the secondary antibodies [goat anti-mouse HRP conjugate (170–6516, Bio-Rad) or goat anti-rabbit HRP conjugate (170–6515, Bio-Rad)] and developed with an ECL solution.

Statistics

We determined *P*-values by a two-tailed Student's *t*-test, assuming equal variance ($^{*}P < 0.05$, $^{**}P < 0.01$ and $^{***}P < 0.001$). We considered differences between groups significant at $P < 0.05$.

SUPPLEMENTARY MATERIAL

Supplementary Material is available at *HMG* online.

ACKNOWLEDGEMENTS

We would like to thank E. Compe (IGBMC, Strasbourg, France) for providing the murine brains for NB experiments. We are grateful to C. Bellemer and J. Cavaillé (IBCG, Toulouse, France) for help with the RNA FISH experiments. We are thankful to the Henry-Henras team (IBCG, Toulouse, France) for providing the anti-fibrillarin antibody. We are indebted to all the members of the team of G.G.-M. for helpful discussions. This work benefited from the TRI Optical Imaging Platform at IPBS (Genotoul, Toulouse, France).

Conflict of Interest statement. None declared.

FUNDING

This work was supported by Région Midi-Pyrénées (grant number 08017067 to J.N.), Fondation pour la Recherche Médicale (grant number FDT20120925285/086257 to J.N.), La Ligue Nationale Contre le Cancer (grant number 062508 to C.B.), ANR (grant number ANR10-BLAN-123101-01 to J.N., C.B., G.G.-M.) and ATIP plus (ATIP AVENIR 2011 Cancer, grant number 201204/080192 to J.N., C.B., G.G.-M.).

REFERENCES

1. Grummt, I. and Voit, R. (2010) Linking rDNA transcription to the cellular energy supply. *Cell Cycle*, **9**, 225–226.
2. Zurita, M. and Merino, C. (2003) The transcriptional complexity of the TFIIH complex. *Trends Genet.*, **19**, 578–584.
3. Giglia-Mari, G., Coin, F., Ranish, J.A., Hoogstraten, D., Theil, A., Wijgers, N., Jaspers, N.G., Raams, A., Argentini, M., van der Spek, P.J *et al.* (2004) A new, tenth subunit of TFIIH is responsible for the DNA repair syndrome trichothiodystrophy group A. *Nat. Genet.*, **36**, 714–719.
4. Rossignol, M., Kolb-Cheynel, I. and Egly, J.M. (1997) Substrate specificity of the cdk-activating kinase (CAK) is altered upon association with TFIIH. *EMBO J.*, **16**, 1628–1637.
5. Schaeffer, L., Moncollin, V., Roy, R., Staub, A., Mezzina, M., Sarasin, A., Weeda, G., Hoeijmakers, J.H. and Egly, J.M. (1994) The ERCC2/DNA repair protein is associated with the class II BTF2/TFIIH transcription factor. *EMBO J.*, **13**, 2388–2392.
6. Schaeffer, L., Roy, R., Humbert, S., Moncollin, V., Vermeulen, W., Hoeijmakers, J.H., Chambon, P. and Egly, J.M. (1993) DNA repair helicase: a component of BTF2 (TFIIH) basic transcription factor. *Science*, **260**, 58–63.
7. Compe, E. and Egly, J.M. (2012) TFIIH: when transcription met DNA repair. *Nat. Rev. Mol. Cell Biol.*, **13**, 343–354.
8. Hoogstraten, D., Nigg, A.L., Heath, H., Mullenders, L.H., van Driel, R., Hoeijmakers, J.H., Vermeulen, W. and Houtsmuller, A.B. (2002) Rapid switching of TFIIH between RNA polymerase I and II transcription and DNA repair in vivo. *Mol. Cell*, **10**, 1163–1174.
9. Iben, S., Tschochner, H., Bier, M., Hoogstraten, D., Hozak, P., Egly, J.M. and Grummt, I. (2002) TFIIH plays an essential role in RNA polymerase I transcription. *Cell*, **109**, 297–306.
10. Andersen, J.S., Lyon, C.E., Fox, A.H., Leung, A.K., Lam, Y.W., Steen, H., Mann, M. and Lamond, A.I. (2002) Directed proteomic analysis of the human nucleolus. *Curr. Biol.*, **12**, 1–11.
11. Assfalg, R., Lebedev, A., Gonzalez, O.G., Schelling, A., Koch, S. and Iben, S. (2011) TFIIH is an elongation factor of RNA polymerase I. *Nucleic Acids Res.*, **40**, 650–659.
12. Moss, T. (2004) At the crossroads of growth control; making ribosomal RNA. *Curr. Opin. Genet. Dev.*, **14**, 210–217.
13. Cisterna, B. and Biggiogera, M. (2010) Ribosome biogenesis: from structure to dynamics. *Int. Rev. Cell Mol. Biol.*, **284**, 67–111.
14. Henras, A.K., Soudet, J., Gerus, M., Lebaron, S., Caizergues-Ferrer, M., Mougin, A. and Henry, Y. (2008) The post-transcriptional steps of eukaryotic ribosome biogenesis. *Cell. Mol. Life Sci.*, **65**, 2334–2359.
15. Fromont-Racine, M., Senger, B., Saveanu, C. and Fasiolo, F. (2003) Ribosome assembly in eukaryotes. *Gene*, **313**, 17–42.
16. Boisvert, F.M., van Koningsbruggen, S., Navascues, J. and Lamond, A.I. (2007) The multifunctional nucleolus. *Nat. Rev. Mol. Cell Biol.*, **8**, 574–585.
17. Casafont, I., Navascues, J., Pena, E., Lafarga, M. and Berciano, M.T. (2006) Nuclear organization and dynamics of transcription sites in rat sensory ganglia neurons detected by incorporation of 5′-fluorouridine into nascent RNA. *Neuroscience*, **140**, 453–462.

18. Freed, E.F., Bleichert, F., Dutca, L.M. and Baserga, S.J. (2010) When ribosomes go bad: diseases of ribosome biogenesis. *Mol. Biosyst.*, **6**, 481–493.
19. Boria, I., Garelli, E., Gazda, H.T., Aspesi, A., Quarello, P., Pavesi, E., Ferrante, D., Meerpohl, J.J., Kartal, M., Da Costa, L *et al.* (2010) The ribosomal basis of Diamond-Blackfan anemia: mutation and database update. *Hum. Mutat.*, **31**, 1269–1279.
20. Choesmel, V., Bacqueville, D., Rouquette, J., Noaillac-Depeyre, J., Fribourg, S., Cretien, A., Leblanc, T., Tchernia, G., Da Costa, L. and Gleizes, P.E. (2007) Impaired ribosome biogenesis in Diamond-Blackfan anemia. *Blood*, **109**, 1275–1283.
21. Devlin, E.E., Dacosta, L., Mohandas, N., Elliott, G. and Bodine, D.M. (2010) A transgenic mouse model demonstrates a dominant negative effect of a point mutation in the RPS19 gene associated with Diamond-Blackfan anemia. *Blood*, **116**, 2826–2835.
22. Jaako, P., Flygare, J., Olsson, K., Quere, R., Ehinger, M., Henson, A., Ellis, S., Schambach, A., Baum, C., Richter, J. *et al.* (2011) Mice with ribosomal protein S19 deficiency develop bone marrow failure and symptoms like patients with Diamond-Blackfan anemia. *Blood*, **118**, 6087–6096.
23. Kraemer, K.H., Patronas, N.J., Schiffmann, R., Brooks, B.P., Tamura, D. and DiGiovanna, J.J. (2007) Xeroderma pigmentosum, trichothiodystrophy and Cockayne syndrome: a complex genotype-phenotype relationship. *Neuroscience*, **145**, 1388–1396.
24. Broughton, B.C., Berneburg, M., Fawcett, H., Taylor, E.M., Arlett, C.F., Nardo, T., Stefanini, M., Menefee, E., Price, V.H., Queille, S *et al.* (2001) Two individuals with features of both xeroderma pigmentosum and trichothiodystrophy highlight the complexity of the clinical outcomes of mutations in the XPD gene. *Hum. Mol. Genet.*, **10**, 2539–2547.
25. Sanij, E. and Hannan, R.D. (2009) The role of UBF in regulating the structure and dynamics of transcriptionally active rDNA chromatin. *Epigenetics*, **4**, 374–382.
26. Hadjiolova, K.V., Hadjiolov, A.A. and Bachellerie, J.P. (1995) Actinomycin D stimulates the transcription of rRNA minigenes transfected into mouse cells. Implications for the in vivo hypersensitivity of rRNA gene transcription. *Eur. J. Biochem.*, **228**, 605–615.
27. Cui, C. and Tseng, H. (2004) Estimation of ribosomal RNA transcription rate in situ. *Biotechniques*, **36**, 134–138.
28. Titov, D.V., Gilman, B., He, Q.L., Bhat, S., Low, W.K., Dang, Y., Smeaton, M., Demain, A.L., Miller, P.S., Kugel, J.F *et al.* (2011) XPB, a subunit of TFIIH, is a target of the natural product triptolide. *Nat. Chem. Biol.*, **7**, 182–188.
29. Bradsher, J., Auriol, J., Proietti de Santis, L., Iben, S., Vonesch, J.L., Grummt, I. and Egly, J.M. (2002) CSB is a component of RNA pol I transcription. *Mol. Cell*, **10**, 819–829.
30. Lebedev, A., Scharffetter-Kochanek, K. and Iben, S. (2008) Truncated Cockayne syndrome B protein represses elongation by RNA polymerase I. *J. Mol. Biol.*, **382**, 266–274.
31. van der Horst, G.T., van Steeg, H., Berg, R.J., van Gool, A.J., de Wit, J., Weeda, G., Morreau, H., Beems, R.B., van Kreijl, C.F., de Gruijl, F.R *et al.* (1997) Defective transcription-coupled repair in Cockayne syndrome B mice is associated with skin cancer predisposition. *Cell*, **89**, 425–435.
32. de Boer, J., de Wit, J., van Steeg, H., Berg, R.J., Morreau, H., Visser, P., Lehmann, A.R., Duran, M., Hoeijmakers, J.H. and Weeda, G. (1998) A mouse model for the basal transcription/DNA repair syndrome trichothiodystrophy. *Mol. Cell*, **1**, 981–990.
33. Andressoo, J.O., Mitchell, J.R., de Wit, J., Hoogstraten, D., Volker, M., Toussaint, W., Speksnijder, E., Beems, R.B., van Steeg, H., Jans, J *et al.* (2006) An Xpd mouse model for the combined xeroderma pigmentosum/Cockayne syndrome exhibiting both cancer predisposition and segmental progeria. *Cancer Cell*, **10**, 121–132.
34. Pestov, D.G., Lapik, Y.R. and Lau, L.F. (2008) Assays for ribosomal RNA processing and ribosome assembly. *Curr. Protoc. Cell Biol.*, **Chapter 22**, Unit 22.11.
35. Mullineux, S.T. and Lafontaine, D.L. (2012) Mapping the cleavage sites on mammalian pre-rRNAs: where do we stand? *Biochimie*, **94**, 1521–1532.
36. Kopp, K., Gasiorowski, J.Z., Chen, D., Gilmore, R., Norton, J.T., Wang, C., Leary, D.J., Chan, E.K., Dean, D.A. and Huang, S. (2007) Pol I transcription and pre-rRNA processing are coordinated in a transcription-dependent manner in mammalian cells. *Mol. Biol. Cell*, **18**, 394–403.
37. Giglia-Mari, G., Theil, A.F., Mari, P.O., Mourgues, S., Nonnekens, J., Andrieux, L.O., de Wit, J., Miquel, C., Wijgers, N., Maas, A *et al.* (2009) Differentiation driven changes in the dynamic organization of basal transcription initiation. *PLoS Biol.*, **7**, e1000220.
38. Dundr, M., Hoffmann-Rohrer, U., Hu, Q., Grummt, I., Rothblum, L.I., Phair, R.D. and Misteli, T. (2002) A kinetic framework for a mammalian RNA polymerase in vivo. *Science*, **298**, 1623–1626.
39. Coin, F., Oksenych, V. and Egly, J.M. (2007) Distinct roles for the XPB/p52 and XPD/p44 subcomplexes of TFIIH in damaged DNA opening during nucleotide excision repair. *Mol. Cell*, **26**, 245–256.
40. Dubaele, S., Proietti De Santis, L., Bienstock, R.J., Keriel, A., Stefanini, M., Van Houten, B. and Egly, J.M. (2003) Basal transcription defect discriminates between xeroderma pigmentosum and trichothiodystrophy in XPD patients. *Mol. Cell*, **11**, 1635–1646.
41. Granneman, S. and Baserga, S.J. (2005) Crosstalk in gene expression: coupling and co-regulation of rDNA transcription, pre-ribosome assembly and pre-rRNA processing. *Curr. Opin. Cell Biol.*, **17**, 281–286.
42. Schneider, D.A., Michel, A., Sikes, M.L., Vu, L., Dodd, J.A., Salgia, S., Osheim, Y.N., Beyer, A.L. and Nomura, M. (2007) Transcription elongation by RNA polymerase I is linked to efficient rRNA processing and ribosome assembly. *Mol. Cell*, **26**, 217–229.
43. Compe, E., Malerba, M., Soler, L., Marescaux, J., Borrelli, E. and Egly, J.M. (2007) Neurological defects in trichothiodystrophy reveal a coactivator function of TFIIH. *Nat. Neurosci.*, **10**, 1414–1422.
44. Jaarsma, D., van der Pluijm, I., de Waard, M.C., Haasdijk, E.D., Brandt, R., Vermeij, M., Rijksen, Y., Maas, A., van Steeg, H., Hoeijmakers, J.H *et al.*. (2011) Age-related neuronal degeneration: complementary roles of nucleotide excision repair and transcription-coupled repair in preventing neuropathology. *PLoS Genet.*, **7**, e1002405.
45. Sambrook, J. and Russell, D.W. (2006) Separation of RNA according to size: electrophoresis of glyoxylated RNA through agarose gels. *CSH Protoc.*, **2006**.